Title:

A 14-channel 7 GHz VCO-based EPR-on-a-chip sensor with rapid scan capabilities

Author(s):
Mohamed Atef Hassan, Tarek Elrifai, Ayman Sakr, Michal Kern, Klaus Lips, and Jens Anders

Citation:

"M. A. Hassan, T. Elrifai, A. Sakr, M. Kern, K. Lips and J. Anders, "A 14-channel 7 GHz VCO-based EPR-on-a-chip sensor with rapid scan capabilities," 2021 IEEE Sensors, 2021, pp. 1-4, doi: 10.1109/SENSORS47087.2021.9639513"
Archiviert unter http://dx.doi.org/10.17169/refubium-34120

A 14-channel 7 GHz VCO-based EPR-on-a-chip sensor with rapid scan capabilities

Mohamed Atef Hassan[1], Tarek Elrifai[1], Ayman Sakr[1], Michal Kern[1], Klaus Lips[2], and Jens Anders[1]
[1]University of Stuttgart, Institute of Smart Sensors, Pffafenwaldring 47, Stuttgart, Germany
[2]Helmholtz Center for Energy and Materials, Berlin, Germany
Email: mohamed.hassan@iis.uni-stuttgart.de jens.anders@iis.uni-stuttgart.de

***Abstract*— This paper presents a VCO-based EPR-on-a-chip (EPRoC) sensor for portable, battery-operated electron paramagnetic resonance (EPR) spectrometers. The proposed chip contains an array of 14 injection-locked VCOs as the sensing element for an improved sensitive volume and phase noise performance. By co-integrating a high-bandwidth PLL, the presented design allows for continuous-wave and rapid-scan EPR experiments with a minimum number of external components. The active loop filter introduces an assisted replica charge pump that mitigates the slewing requirements on the loop-filter amplifier. The measured spin sensitivity of 2×10^9 spins/$\sqrt{\text{Hz}}$ together with the large active volume of 210 nl lead to an 8-fold improvement in concentration sensitivity compared to the state-of-the-art in EPRoC detectors.**

Keywords—EPR, EPR-on-a-chip, EPRoC, PLL, Charge pump, Injection-locked, SOI.

I. Introduction

Electron paramagnetic resonance (EPR) spectroscopy and imaging are the gold standards for detecting paramagnetic species such as free radicals, which play an important role in medicine, where they critically determine the difference between a healthy physiological state and a pathological condition [1]. Moreover, paramagnetic states critically affect the performance and state-of-health of many modern energy storage devices [2].

Conventional EPR spectrometers are bulky and expensive devices, preventing the widespread use of EPR. To overcome this problem, in [3], a new approach for detecting the EPR effect was proposed. In this approach, a CMOS voltage-controlled oscillator (VCO) was used to both excite and detect the EPR signal. The wide-range frequency sweeps with a near-constant sensitivity enabled by the VCO-based approach allowed to replace the bulky, power-hungry, and expensive electromagnet of conventional EPR setups, enabling the design of the first battery-operated, point-of-care EPR spectrometer. In [1], this EPR-on-a-chip (EPRoC) approach was further improved by using an array of injection-locked VCOs. Together with the positive effect of injection locking on the phase noise of the array, the greatly increased sensitive volume of this design drastically improved the concentration sensitivity of the presented spectrometer to a value of 200 µM/$\sqrt{\text{Hz}}$ [1]. However, physiologically relevant concentrations of free radicals are typically in the single-digit µM or upper nM range, requiring further significant sensitivity improvements to the EPRoC approach.

This work has been supported by the Bundesministerium für Bildung und Forschung under contract number 01186916/1 (EPRoC).

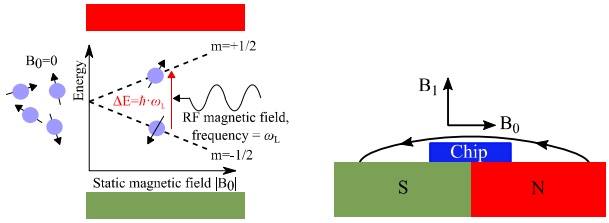

(a) (b)

Fig. 1. a) Principle of operation of EPR and b) a single-sided spectrometer.

Furthermore, the design in [1] required off-chip frequency demodulation, increasing the overall system complexity. This paper presents a 14-channel VCO-based EPRoC detector that incorporates an on-chip, high-bandwidth (BW) phase-locked-loop (PLL) for reduced overall system complexity. The EPRoC approach is ideally suited for integration with single-sided magnets, which provide optimum sample access from the top, cf. Fig. 1b. The presented design extends the state-of-the-art in EPRoC devices [1, 4] in several aspects: By increasing the array size from 8 [1] to 14 VCOs, the sensitive volume is almost doubled. Next, by co-integrating a high-BW PLL together with the injection-locked VCO array, the VCO frequency can be derived from a well-defined external reference. Moreover, the PLL provides on-chip demodulation of the EPR signal while keeping the external component count at a minimum. Compared to [4], the reduced parasitics of the on-chip PLL can be leveraged to achieve a greatly improved PLL BW, enabling more advanced EPR detection schemes such as rapid-scan (RS) measurements. RS EPR has recently gained significant interest in the EPR community since it allows for improved sensitivities compared to conventional continuous wave (CW) measurements [5]. In contrast to conventional RS EPR, the VCO-based EPRoC approach uses fast frequency sweeps instead of fast magnetic field sweeps, rendering it compatible with permanent magnets and battery operation.

II. EPR Theory of Operation

EPR makes use of the spin of unpaired electrons as they occur, e. g., in free radicals, and are associated with many defects in solid-state materials. The energy state of the electron spin is degenerate in the absence of a magnetic field. However, if a static magnetic field B_0 is applied, it splits into two discrete energy states (Zeeman effect) with an energy difference of:

$$\Delta E = \hbar \cdot \gamma \cdot B_0 = \hbar \cdot \omega_L, \quad (1)$$

where $\hbar$ is the reduced Planck constant, γ is the gyromagnetic ratio ($\gamma \approx 2\pi \cdot 28$ GHz/T for free electrons), and ω_L is the so-called Larmor frequency. By applying a microwave magnetic field B_1, whose frequency is sufficiently close to the Larmor

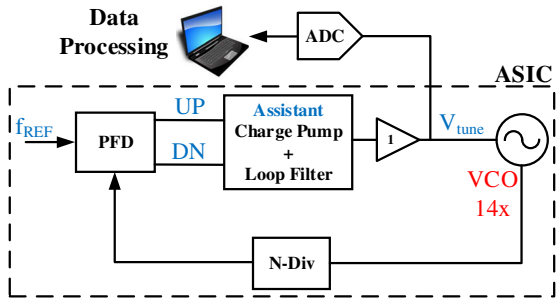

Fig. 2. Architecture of the presented systems.

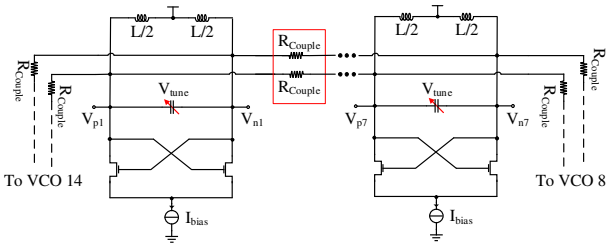

Fig. 3. Schematic of the injection-locked 14-VCO array.

frequency, transitions between the two energy states can be induced, cf. Fig. 1a, which produces a change in the net sample magnetization. In conventional EPR, the sample is placed inside a microwave resonator, and the EPR effect is detected as a change in the reflected power when irradiating the sample with a constant microwave frequency ω_{MW} and sweeping the static field B_0 through the resonance condition $\omega_{MW} \approx \omega_L = \gamma \cdot B_0$. The achievable limit of detection is typically improved by modulating the B_0 field to allow for lock-in detection. Overall, this resonator-based detection principle prevents frequency-swept experiments due to the large resonator quality factor that is needed to achieve good sensitivity. Therefore, resonator-based EPR requires bulky and power-hungry electromagnets, rendering the miniaturization of conventional EPR setups difficult.

To solve this problem, in [3], the concept of VCO-based EPR was introduced. Here, the sample is placed on top of the coil of a monolithic LC VCO. In this approach, the current running through said coil produces the B_1-field exciting the electrons, and the resulting change in magnetization is detected as a change in oscillation frequency, cf. Fig. 1b. An EPR experiment is performed by sweeping the VCO tuning voltage and recording the EPR-induced difference from its nominal tuning characteristic. Alternatively, one can embed the VCO into a PLL. In this configuration, an EPR experiment is performed by sweeping the VCO frequency through the resonance condition and recording the PLL tuning voltage [4]. Inside the PLL BW, the EPR signal induced in the coil is translated into a corresponding change in said tuning voltage, providing an implicit FM demodulation of the EPR signal. By modulating the PLL reference, FM-based lock-in detection for sensitivity enhancement can be conveniently implemented in this scheme. Overall, VCO-based detection allows for frequency-swept EPR experiments with near-constant sensitivity since the VCO is intrinsically tuned to the correct excitation frequency. This, in turn, enables the use of fixed B_0 fields that can easily be produced by miniaturized permanent magnets to form compact and portable EPR sensors, cf. Fig. 1b and [3]. Moreover, frequency-swept EPR with VCO-based

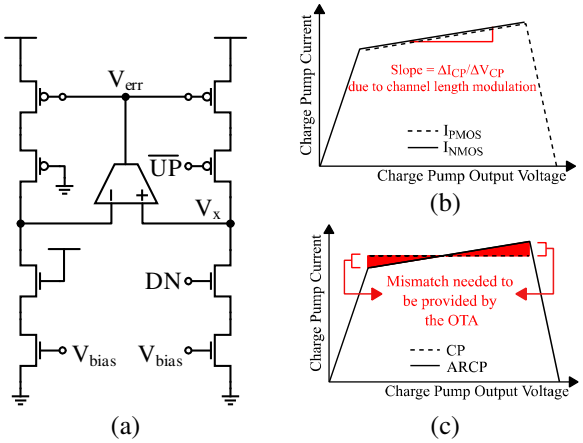

Fig. 4. (a) Conventional CP mismatch compensation, (b) corresponding CP current vs. output voltage, (c) and CP current vs. output voltage of the proposed CP in Fig. 5.

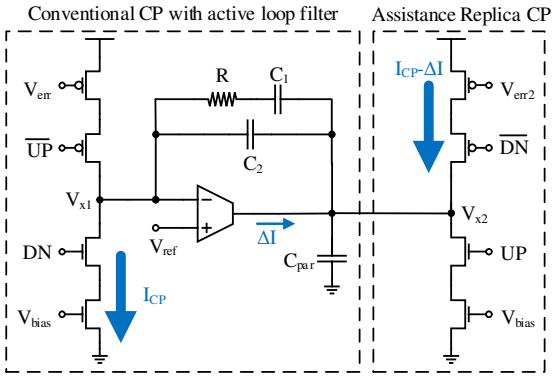

Fig. 5. Active loop filter with the proposed ARCP.

detectors drastically facilitates RS EPR experiments, which have recently gained popularity as an efficient measure to boost sensitivity [5]. More specifically, while in conventional RS EPR experiments, modulation coils with large inductances are used to conduct fast magnetic field sweeps, VCO-based EPRoC uses fast frequency chirps. Such frequency chirps can be produced on-chip in a very power-efficient way using highly linear, high-BW PLLs for excitation and signal demodulation. The corresponding PLL design will be discussed in detail in section III.B.

III. Architecture

A. VCO Array

Fig. 2 shows the block diagram of the proposed EPR sensor, highlighting the high level of integration of the presented approach. The EPRoC sensor is realized as an array of 14 injection-locked LC tank VCOs, connected in a ring configuration using resistors for injection locking, cf. Fig. 3, with large-diameter tank coils (d_{coil} = 210 µm) to provide an increased sensitive volume and, thus, improved concentration sensitivity compared to the state-of-the-art in [1]. Overall, compared to [1], the array has approximately twice the sensitive volume. To be compatible with single-sided magnets placed directly underneath the chip, which allows for the formation of very compact sensor systems, the operating frequency has been reduced to 7 GHz. This corresponds to a magnetic field of approximately 250 mT, which can well be realized with single-sided magnets. The

resulting theoretical loss of $2^{3/2}$ in spin sensitivity compared to the 14 GHz design in [1] is partially compensated by the lower phase noise of the individual 7 GHz VCOs and the larger number of injection-locked VCOs, which furthers lowers the phase noise of the joint array frequency by approximately 30%.

B. *High-BW PLL for CW and RS EPR*

The VCO array is controlled by a single on-chip, integer-N, charge-pump (CP) PLL to avoid the noise penalty of a fractional-N PLL with a BW as large as 20 MHz. The PLL uses a mismatch compensated CP, cf. Fig. 4a, a second-order active loop filter according to Fig. 5, and division factor of 16.

Active Loop Filter with Assisted Replica Charge Pump

RS measurements require sweeping the VCO frequency across a large fraction of the VCO tuning range using fast triangular waveforms. In an integer-N PLL, this is achieved by modulating the PLL reference accordingly. The result is a corresponding triangular waveform on the PLL tuning voltage V_{tune}. To maintain the BW and the phase margin of the PLL over the wide output range, the CP output current has to be kept constant over the triangular chirp in the presence of the typical circuit nonidealities of charge-pump-loop-filter combinations.

Additionally, CPs suffer from a current mismatch between the NMOS and PMOS branches. In [6], a feedback loop is used to match the PMOS branch to the NMOS, effectively eliminating the mismatch cf. Fig. 4a. However, channel length modulation of the unregulated NMOS transistors, cf. Fig. 4b, still affects the PLL dynamic range and linearity. In [7], an active loop filter is used to maintain the charge pump output voltage at a constant level, essentially reducing the operating range along the curve in Fig. 4b to a single point. However, this poses stringent requirements on the amplifier used in the loop filter. The amplifier not only requires a high BW to preserve the phase margin but also has to supply sharp current pulses at a rate equal to the reference frequency. Especially the high slewing requirement poses a challenge when designing an active loop filter for high BW PLLs with correspondingly large reference frequencies.

In the proposed design, we combine the techniques of [6] and [7] with a new active loop filter that incorporates an assistance technique similar to the one introduced in the context of ΣΔ modulators in [8]. Fig. 5 shows the proposed active loop filter structure. It includes an assisted replica charge pump (ARCP) at the output of the active filter that greatly alleviates the slewing requirements of the amplifier. The CP and the ARCP are individually biased by two feedback loops according to Fig. 4a. To keep the virtual ground node V_{x1} constant, a current pulse equal to that of the CP has to be provided through the loop filter. Without the ARCP, this current would be supplied by the amplifier, leading to the high slewing requirements mentioned above. In the proposed scheme, the ARCP supplies the required current pulses. By carefully matching the two CPs, the amplifier needs to provide only the relatively small current mismatch between the two CPs, cf. Fig. 4c, greatly relaxing the requirements of the amplifier. The residual error is mostly due to channel length modulation of the NMOS branch in the ARCP. The proposed scheme allows extending the techniques of [6] and [7] to higher reference frequencies and, therefore, higher PLL BWs. For a CP output range between 0.4 V and 1.4 V and a CP current of 1 mA, simulations show that the maximum expected (3σ variations) current mismatch between the two CPs is 200 µA. To provide the corresponding current pulses in an energy-efficient way, the loop filter amplifier is implemented as a symmetrical OTA with an adaptive biasing scheme using flipped voltage followers for its input stage.

To account for the large parasitic capacitances of the array at its control input and the off-chip connection of the tuning voltage (pad, PCB trace, and ADC input capacitance), cf. Fig. 2, a buffer is inserted between the output of the ARCP and the array tuning voltage. The noise requirements of the loop filter OTA and the buffer amplifier are relaxed by the PLL loop gain according to:

$$V^2_{\text{n,tune}}(f) \approx \left(\frac{4\pi^2 N f}{I_{\text{CP}} Z_{\text{LF}}(f) K_{\text{VCO}}}\right)^2 \left(V^2_{\text{n,OTA}}(f) + V^2_{\text{n,buf}}(f)\right) \quad (2)$$

where $V^2_{\text{n,tune}}$ is the noise referred to the VCO control node, $Z_{\text{LF}}(f)$ is the impedance of the passive network in the OTA feedback, cf. Fig. 5, N is the PLL division factor, $V^2_{\text{n,OTA}}(f)$ is the output-referred noise of the OTA and $V^2_{\text{n,buf}}(f)$ is the input-referred noise of the buffer.

IV. Measurement Results

A chip micrograph of the presented EPRoC sensor is shown in Fig. 6. The chip is fabricated in a 180 nm SOI CMOS technology and consumes 376 mW of power from a 2-V supply for the VCO array and a 1.8-V supply for the PLL. The measured PLL BW is 20 MHz. The frequency noise floor as a function of the frequency deviation of the FM modulated

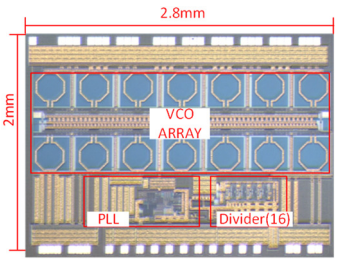

Fig. 6. Chip micrograph of the EPRoC sensor.

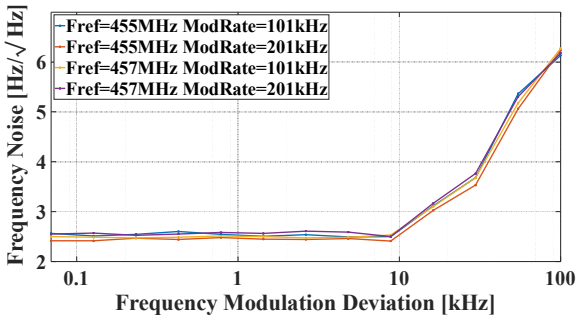

Fig. 7. Frequency noise of the array vs. FM deviation of the FM modulation of the PLL reference.

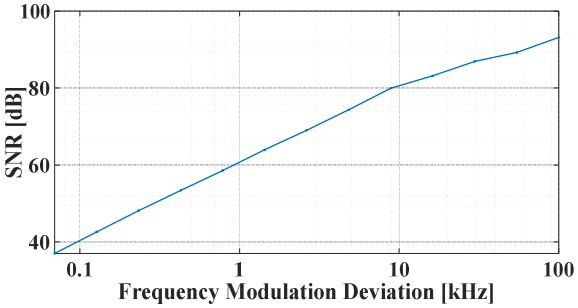

Fig. 8. Dynamic range plot of the presented EPRoC sensor.

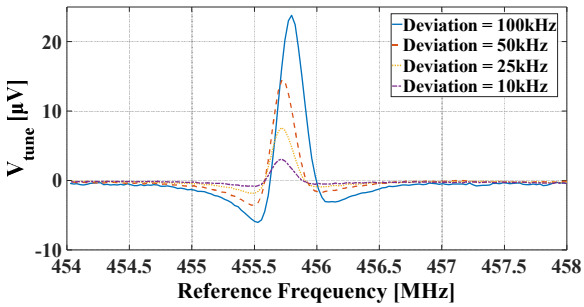

Fig. 9. Measured CW EPR spectrum of BDPA.

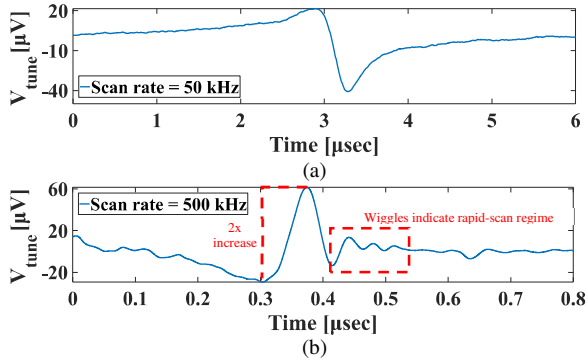

Fig. 10. Measured RS spectra of a BDPA sample at scan rates of a) 50 kHz and b) 500 kHz.

PLL reference and dynamic range of the sensor were electrically characterized. The corresponding results are shown in Figs. 7 and 8. The measured frequency noise floor and dynamic range are 2.5 Hz/$\sqrt{\text{Hz}}$ and 80 dB, respectively. For FM deviations larger than 10 kHz, noise-folding due to the nonlinearity of the VCO tuning curve start to degrade the noise floor and affect the slope of the dynamic range plot.

A. *Continuous-wave EPR Measurements*

All CW EPR experiments have been performed with a frequency modulation of the PLL reference signal and a digital lock-in amplifier connected to the tuning voltage of the VCO array. To characterize the spin sensitivity of our system, we have used BDPA (sample volume: 9 pl), a commonly used EPR standard. Fig. 9 shows the corresponding EPR spectra for a modulation rate of 101 kHz and different frequency deviations. From these experiments, we have determined a spin sensitivity of 2×10^9 spins/$\sqrt{\text{Hz}}$. This corresponds to 4x and 2x improvements compared to [1] and [3]. Together with the 2x and 8x increased sensitive volumes, this leads to 8x and 16x improvement in concentration sensitivity compared to [1] and [3], respectively.

B. *Rapid-scan EPR Measurements*

For RS measurements, the sensor output is connected to an off-chip highspeed ADC. A linear frequency chirp has been applied to the PLL reference input. Fig. 10 shows the corresponding EPR spectra after baseline subtraction. The wiggles indicate the RS regime, which is entered for repetition rates of the triangular frequency signal greater than approximately 200 kHz. Thanks to the fast sweep rate, the EPR signal saturates at higher excitation powers, leading to a 2-fold increase in signal amplitude from the CW regime (50 kHz scan rate) to the RS regime (500 kHz scan rate).

V. Conclusion

In this paper, we have presented a chip-integrated VCO-based EPR detector that incorporates a high-BW PLL for implicit demodulation of the EPR signal in both CW and RS EPR experiments. The sensor performance is compared against the state-of-the-art in EPRoC detectors in Table I. Overall, with its improved concentration sensitivity and high degree of integration, the presented EPRoC detector paves the way towards low-cost, portable EPR spectrometers with sensitivities sufficient for the detection of physiological concentrations of free radicals in personalized medicine.

TABLE I. Comparison against the state-of-the-art

	This work	**[1]**	**[3]**	**[9]**	**[10]**
Field	0.25 T	0.5 T	0.5 T	32mT	0.5 T
Frequency range [GHz]	7.2-7.4	11.8-14.2	13.2-14.3	0.895-0.979	11.2-14.5
Spin sensitivity [spins/√Hz]	2×10^9	8×10^9	4×10^9	1.4×10^{18}	6.1×10^8
Normalized spin sensitivity [spins·$T^{3/2}$/√Hz]	2.5×10^8	2.8×10^9	1.4×10^9	8×10^{15}	2.2×10^8
Sensitive Volume	210 nl	120 nl	27 nl	10 µl	7.5 nl
Power [mW]	20/ch	15/ch	15	–	1.12[a]
Level of integration	Very high	High	High	High	High
Technology	0.18µm CMOS	0.13µm CMOS	0.13µm CMOS	0.13µm BiCMOS	28nm CMOS

[a] 14 GHz excitation source off-chip

References

[1] A. Chu, B. Schlecker, K. Lips, M. Ortmanns, and J. Anders, "An 8-channel 13GHz ESR-on-a-Chip injection-locked vco-array achieving 200µM-concentration sensitivity," *2018 IEEE International Solid-State Circuits Conference (ISSCC)*, San Francisco, CA, USA, 2018, pp. 354-356.

[2] S. Steffens et al., "Impact of dislocations and dangling bond defects on the electrical performance of crystalline silicon thin films", Applied Physics Letters, vol. 105, 2014.

[3] J. Handwerker et al., "A 14GHz battery-operated point-of-care ESR spectrometer based on a 0.13µm CMOS ASIC," *2016 IEEE International Solid-State Circuits Conference (ISSCC)*, San Francisco, CA, USA, 2016, pp. 476-477.

[4] B. Schlecker et al., "Towards Low-Cost, High-Sensitivity Point-of-Care Diagnostics Using VCO-Based ESR-on-a-Chip Detectors," in *IEEE Sensors Journal*, vol. 19, no. 20, pp. 8995-9003, 2019.

[5] J. Möser et al., "Using rapid-scan EPR to improve the detection limit of quantitative EPR by more than one order of magnitude", *Journal of Magnetic Resonance*, vol. 281, pp. 17-25, 2017.

[6] Hwang, M.-S.; Kim, J., and Jeong, D.-K., "Charge pump with perfect current matching characteristics in phase-locked loops", *Electronics Letters*, vol. 36, no. 23, p. 135-136, 2000.

[7] Li Lin, L. Tee, and P. R. Gray, "A 1.4 GHz differential low-noise CMOS frequency synthesizer using a wideband PLL architecture," *2000 IEEE International Solid-State Circuits Conference (ISSCC)*, San Francisco, CA, USA, 2000, pp. 204-205.

[8] S. Pavan and P. Sankar, "Power Reduction in Continuous-Time Delta-Sigma Modulators Using the Assisted Opamp Technique," in *IEEE Journal of Solid-State Circuits*, vol. 45, no. 7, pp. 1365-1379, July 2010.

[9] X. Yang and A. Babakhani, "A Single-Chip Electron Paramagnetic Resonance Transceiver in 0.13-µm SiGe BiCMOS," in *IEEE Transactions on Microwave Theory and Techniques*, vol. 63, no. 11, pp. 3727-3735, Nov. 2015.

[10] L. Zhang and A. M. Niknejad, "An Ultrasensitive 14-GHz 1.12-mW EPR Spectrometer in 28-nm CMOS," in *IEEE Microwave and Wireless Components Letters,* 2021.